

First observation of correlations between spin and transverse momenta in back-to-back dihadron production at CLAS12

H. Avakian,¹ T.B. Hayward,² A. Kotzinian,^{3,4} W.R. Armstrong,⁵ H. Atac,⁶ C. Ayerbe Gayoso,⁷ L. Baashen,⁸
N.A. Baltzell,¹ L. Barion,⁹ M. Bashkanov,¹⁰ M. Battaglieri,¹¹ I. Bedlinskiy,¹² B. Benkel,¹³ F. Benmokhtar,¹⁴
A. Bianconi,^{15,16} L. Biondo,^{11,17,18} A.S. Biselli,¹⁹ M. Bondi,²⁰ S. Boiarinov,¹ F. Bossù,²¹ K.T. Brinkman,²²
W.J. Briscoe,²³ W.K. Brooks,¹³ S. Bueltmann,²⁴ D. Bulumulla,²⁴ V.D. Burkert,¹ R. Capobianco,²
D.S. Carman,¹ J.C. Carvajal,⁸ A. Celentano,¹¹ P. Chatagnon,²⁵ V. Chesnokov,²⁶ T. Chetry,^{8,27,28} G. Ciullo,^{9,29}
P.L. Cole,³⁰ M. Contalbrigo,⁹ G. Costantini,^{15,16} A. D'Angelo,^{20,31} N. Dashyan,³ R. De Vita,¹¹ M.
Defurne,²¹ A. Deur,¹ S. Diehl,^{22,2} C. Dilks,³² C. Djalali,²⁸ R. Dupre,²⁵ H. Egiyan,¹ A. El Alaoui,¹³
L. El Fassi,²⁷ L. Elouadrhiri,¹ S. Fegan,¹⁰ A. Filippi,⁴ T. Forest,³³ K. Gates,³⁴ G. Gavalian,¹ Y. Ghandilyan,³
D.I. Glazier,³⁴ A.A. Golubenko,²⁶ G. Gosta,^{15,16} R.W. Gothe,³⁵ Y. Gotra,¹ K.A. Griffioen,⁷ M. Guidal,²⁵
H. Hakobyan,¹³ M. Hattawy,²⁴ F. Hauenstein,¹ D. Heddle,^{36,1} A. Hobart,²⁵ M. Holtrop,³⁷ C.E. Hyde,²⁴
Y. Ilieva,³⁵ D.G. Ireland,³⁴ E.L. Isupov,²⁶ H.S. Jo,³⁸ R. Johnston,³⁹ K. Joo,² M.L. Kabir,²⁷ D. Keller,⁴⁰
M. Khachatryan,²⁴ A. Khanal,⁸ A. Kim,² W. Kim,³⁸ V. Klimenko,² A. Kripko,²² V. Kubarovsky,¹
S.E. Kuhn,²⁴ V. Lagerquist,²⁴ L. Lanza,²⁰ M. Leali,^{15,16} S. Lee,³⁹ P. Lenisa,^{9,29} X. Li,³⁹ I. J. D. MacGregor,³⁴
D. Marchand,²⁵ V. Mascagna,^{15,16} B. McKinnon,³⁴ S. Migliorati,^{15,16} T. Mineeva,¹³ M. Mirazita,⁴¹ V. Mokeev,¹
R.A. Montgomery,³⁴ C. Munoz Camacho,²⁵ P. Nadel-Turonski,¹ P. Naidoo,³⁴ K. Neupane,³⁵ D. Nguyen,¹
S. Niccolai,²⁵ M. Nicol,¹⁰ G. Niculescu,⁴² M. Osipenko,¹¹ P. Pandey,²⁴ M. Paolone,^{43,6} L.L. Pappalardo,^{9,29}
R. Paremuzyan,^{1,37} E. Pasyuk,¹ S.J. Paul,⁴⁴ W. Phelps,^{36,23} N. Pilleux,²⁵ O. Pogorelko,¹² M. Pokhrel,²⁴
J. Poudel,²⁴ J.W. Price,⁴⁵ Y. Prok,²⁴ B.A. Raue,⁸ T. Reed,⁸ J. Richards,² M. Ripani,¹¹ J. Ritman,^{46,47}
P. Rossi,^{1,41} F. Sabatié,²¹ C. Salgado,⁴⁸ A. Schmidt,^{23,39} Y.G. Sharabian,¹ E.V. Shirokov,²⁶ U. Shrestha,²
P. Simmerling,² D. Sokhan,^{21,34} N. Sparveris,⁶ S. Stepanyan,¹ I.I. Strakovsky,²³ S. Strauch,³⁵ J.A. Tan,³⁸
N. Trotta,² R. Tyson,³⁴ M. Ungaro,¹ S. Vallarino,⁹ L. Venturelli,^{15,16} H. Voskanyan,³ A. Vossen,^{32,1} E. Voutier,²⁵
D.P. Watts,¹⁰ X. Wei,¹ R. Wishart,³⁴ M.H. Wood,⁴⁹ N. Zachariou,¹⁰ Z.W. Zhao,³² and M. Zurek⁵

(The CLAS Collaboration)

¹Thomas Jefferson National Accelerator Facility, Newport News, Virginia 23606

²University of Connecticut, Storrs, Connecticut 06269

³Yerevan Physics Institute, 375036 Yerevan, Armenia

⁴INFN, Sezione di Torino, 10125 Torino, Italy

⁵Argonne National Laboratory, Argonne, Illinois 60439

⁶Temple University, Philadelphia, PA 19122

⁷College of William and Mary, Williamsburg, Virginia 23187-8795

⁸Florida International University, Miami, Florida 33199

⁹INFN, Sezione di Ferrara, 44100 Ferrara, Italy

¹⁰University of York, York YO10 5DD, United Kingdom

¹¹INFN, Sezione di Genova, 16146 Genova, Italy

¹²National Research Centre Kurchatov Institute - ITEP, Moscow, 117259, Russia

¹³Universidad Técnica Federico Santa María, Casilla 110-V Valparaíso, Chile

¹⁴Duquesne University, 600 Forbes Avenue, Pittsburgh, PA 15282

¹⁵Università degli Studi di Brescia, 25123 Brescia, Italy

¹⁶INFN, Sezione di Pavia, 27100 Pavia, Italy

¹⁷INFN, Sezione di Catania, 95123 Catania, Italy

¹⁸Università degli Studi di Messina, 98166 Messina, Italy

¹⁹Fairfield University, Fairfield CT 06824

²⁰INFN, Sezione di Roma Tor Vergata, 00133 Rome, Italy

²¹IRFU, CEA, Université Paris-Saclay, F-91191 Gif-sur-Yvette, France

²²II. Physikalisches Institut der Universität Gießen, 35392 Gießen, Germany

²³The George Washington University, Washington, DC 20052

²⁴Old Dominion University, Norfolk, Virginia 23529

²⁵Université Paris-Saclay, CNRS/IN2P3, IJCLab, 91405 Orsay, France

²⁶Skobeltsyn Institute of Nuclear Physics, Lomonosov Moscow State University, 119234 Moscow, Russia

²⁷Mississippi State University, Mississippi State, MS 39762-5167

²⁸Ohio University, Athens, Ohio 45701

²⁹Università di Ferrara, 44121 Ferrara, Italy

³⁰Lamar University, 4400 MLK Blvd, PO Box 10046, Beaumont, Texas 77710

³¹Università di Roma Tor Vergata, 00133 Rome Italy

³²*Duke University, Durham, North Carolina 27708-0305*

³³*Idaho State University, Pocatello, Idaho 83209*

³⁴*University of Glasgow, Glasgow G12 8QQ, United Kingdom*

³⁵*University of South Carolina, Columbia, South Carolina 29208*

³⁶*Christopher Newport University, Newport News, Virginia 23606*

³⁷*University of New Hampshire, Durham, New Hampshire 03824-3568*

³⁸*Kyungpook National University, Daegu 41566, Republic of Korea*

³⁹*Massachusetts Institute of Technology, Cambridge, Massachusetts 02139-4307*

⁴⁰*University of Virginia, Charlottesville, Virginia 22901*

⁴¹*INFN, Laboratori Nazionali di Frascati, 00044 Frascati, Italy*

⁴²*James Madison University, Harrisonburg, Virginia 22807*

⁴³*New Mexico State University, PO Box 30001, Las Cruces, NM 88003, USA*

⁴⁴*University of California Riverside, 900 University Avenue, Riverside, CA 92521, USA*

⁴⁵*California State University, Dominguez Hills, Carson, CA 90747*

⁴⁶*GSI Helmholtzzentrum für Schwerionenforschung GmbH, D-64291 Darmstadt, Germany*

⁴⁷*Institute für Kernphysik (Juelich), Juelich, Germany*

⁴⁸*Norfolk State University, Norfolk, Virginia 23504*

⁴⁹*Canisius College, Buffalo, NY*

(Dated: August 6, 2022)

We report the first measurements of deep inelastic scattering spin-dependent azimuthal asymmetries in back-to-back hadron electroproduction, where two hadrons are produced in opposite hemispheres along the z-axis in the center-of-mass frame, with the first hadron produced in the current-fragmentation region and the other in the target-fragmentation region. The data were taken with longitudinally polarized electron beams of energy 10.2 and 10.6 GeV incident on an unpolarized liquid-hydrogen target using the CLAS12 spectrometer at Jefferson Lab. Observed non-zero $\sin \Delta\phi$ modulations in $ep \rightarrow e'p\pi^+X$ events, where $\Delta\phi$ is the difference of the azimuthal angles of the proton and pion in the virtual photon and target nucleon center-of-mass frame, indicate that correlations between the spin and transverse momenta of hadrons produced in the target- and current-fragmentation regions may be significant. The measured beam-spin asymmetries provide a first access in dihadron production to a previously unobserved leading-twist spin- and transverse-momentum-dependent fracture function. The fracture functions describe the hadronization of the target remnant after the hard scattering of a virtual photon off a quark in the target particle and provide a new avenue for studying nucleonic structure and hadronization.

Keywords: dihadron; beam-spin asymmetry; SIDIS; CLAS12; TMD; fracture function; back-to-back; dSIDIS

INTRODUCTION

The quest for a complete understanding of nucleonic structure and the mechanism by which hadrons form out of constituent partons is one of the ultimate goals of nuclear physics. In deep inelastic scattering (DIS) an electron scatters off a nucleon with sufficient energy and momentum transfer that the process is well-described by incoherent scattering from individual partons (quarks or gluons). In semi-inclusive deep inelastic scattering (SIDIS), one or more hadrons are detected in coincidence with the scattered electron, providing information on the initial quark flavor, transverse momentum and spin [1]. The majority of SIDIS studies have focused on the analysis of hadron production in the current-fragmentation region (CFR), where the final-state hadrons are produced from the struck quark. The production of hadrons in the CFR can be described in a factorized framework by the convolution of Parton Distribution Functions (PDFs) and Fragmentation Functions (FFs) [2]. Here the PDFs describe the probability of finding a specific quark or gluon in a particular state inside the nucleon [3, 4] and the FFs dictate the formation of hadrons out of quarks

and gluons [5]. However, hadrons produced in the target-fragmentation region (TFR), formed under the participation of the spectator partons, are not described by this picture and have been largely unexplored until now.

This letter describes the first ever SIDIS detection of a hadron in the CFR (a π^+) in coincidence with a hadron in the TFR (a proton). The corresponding theoretical basis to study the TFR is based on the fracture function formalism and was established in Ref. [6] for the collinear case. This approach has been generalized to the spin and transverse momentum dependent (STMD) case [7]. Similar to the case of PDFs and FFs in the CFR, the fracture functions describe the conditional probability for the target remnant to form a specific final state hadron after the ejection of a particular quark. In electroproduction, the polarization state of the virtual photon depends on the longitudinal polarization of the lepton beam, which in turn selects preferentially one polarization state of the struck quark. The opposite polarization and transverse momentum of the remnant can introduce correlations between final-state hadrons produced in the TFR and hadrons produced in the CFR. The study of this dihadron production in SIDIS with

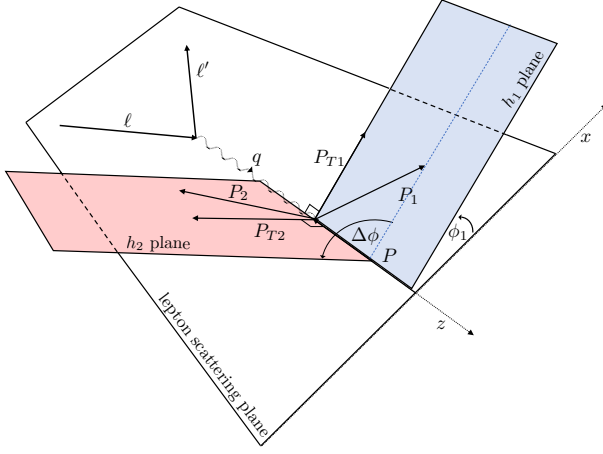


FIG. 1. The SIDIS kinematics of back-to-back dihadron production in the center-of-mass frame. The x - z plane is defined by the incoming and outgoing lepton with positive z in the direction of the virtual photon. ϕ_1 and ϕ_2 are defined from the scattering plane to P_1 and P_2 in an anti-clockwise direction.

a longitudinally polarized electron, where one hadron is produced in the CFR and another in the TFR, provides access to leading twist fracture functions [8]. In the valence-quark region, the polarization transfer from the beam to the active quark is expected to be significant at the relatively low center-of-mass energies accessible at CLAS12 [9]. Preliminary studies using CLAS data indicated that these target-current correlations may be significant [10]. The high luminosity and high polarization of the electron beam along with a wide acceptance for the detection of many final-state particles makes CLAS12 an ideal place for studies of correlations between the target- and current-fragmentation regions.

Sizable beam single-spin asymmetries (SSAs) for a longitudinally polarized electron beam on nucleon targets and one or two hadrons detected in the CFR have been observed at JLab [11–14], HERMES [15] and COMPASS [16–18]. These results have been interpreted in terms of higher twist contributions, related to quark-gluon correlations. Here, higher twist refers to quantities that are suppressed by the hard scale of the process [19]. When one of two hadrons is detected in the TFR and the other in the CFR, the beam SSAs measured here appear at leading twist [20] without this suppression.

In the target fragmentation region it is not possible to separate quark emission from hadron production. This prevents access to a chiral-odd quantity, such as the Collins function, to pair with any chiral-odd fracture functions in single hadron production and ultimately makes any chiral-odd fracture functions inaccessible in single hadron production. In contrast, in the double hadron production process $l(\ell) + N(P) \rightarrow l(\ell') + h_1(P_1) + h_2(P_2) + X$, at perturbative QCD leading order, the cross section expression includes all twist-2 fracture functions

and quark fragmentation functions [7, 8] by pairing the fracture function with a fragmentation function that dictates the production of a hadron in the CFR.

The process considered here is shown in Fig. 1. We use the standard DIS variables: the momentum of the exchanged virtual photon, $q = l - l'$, the scale of the process, $Q^2 = -q^2$, the fractional longitudinal target momentum carried by the struck quark, $x = Q^2/2P \cdot q$, the fractional energy loss of the scattered electron $y = P \cdot q/P \cdot l$ and the hadronic mass of the system, $W^2 = (P + q)^2$. The hadronic variables are defined below. For the case of a longitudinally polarized beam and unpolarized target after the integration over ϕ_2 (the azimuthal angle of the TFR hadron) and keeping $\Delta\phi = \phi_2 - \phi_1$ fixed, there are two contributions to the cross section, σ_{UU} and σ_{LU} [21],

$$\sigma_{UU} = F_0^{\hat{u}_1 \cdot D_1}, \quad (1)$$

$$\sigma_{LU} = \frac{P_{T1} P_{T2}}{m_N m_2} F_{k1}^{\hat{l}_1^{\perp h} \cdot D_1} \sin(\Delta\phi), \quad (2)$$

where the structure functions $F_0^{\hat{u}_1 \cdot D_1}$ and $F_{k1}^{\hat{l}_1^{\perp h} \cdot D_1}$ are convolutions [8] of the leading twist fracture functions \hat{u}_1 and $\hat{l}_1^{\perp h}$ with the unpolarized fragmentation function, D_1 , which depend on the kinematic variables $x, Q^2, z_1, \zeta_2, P_{T1}^2, P_{T2}^2$, and $\vec{P}_{T1} \cdot \vec{P}_{T2}$. The masses of the nucleon target, forward and backward produced hadrons are denoted as m_N, m_1 and m_2 . The hadron 1, h_1 , produced in the CFR ($x_{F1} > 0$)¹ is described by the standard scaled variable $z_1 = P \cdot P_1/P \cdot q$, describing the fraction of the virtual photon energy carried by the CFR hadron, and its transverse momentum \vec{P}_{T1} (defined relative to the q vector in the target rest frame) with magnitude P_{T1} and azimuthal angle ϕ_1 . The hadron 2, h_2 , produced in the TFR ($x_{F2} < 0$) is described by similar variables: the fractional longitudinal target momentum carried by the TFR hadron, $\zeta_2 \simeq E_2/E$ where E is the energy of the target, and \vec{P}_{T2} (P_{T2} and ϕ_2) in the virtual photon and target nucleon center-of-mass frame. The usual hadronic scaling variable, z , is not used in the TFR because of ambiguities between soft hadron emission and target fragmentation [7].

In particular, the structure function in Eq. 2 contains the fracture function $\hat{l}_1^{\perp h}(\zeta_2, P_{T2})$, describing the production of h_2 after the emission of a longitudinally polarized quark in an unpolarized nucleon and $D_1(z_1, P_{T1})$, the unpolarized fragmentation function describing the formation of h_1 . This structure function depends on the relative azimuthal angle of the two hadrons, indicating a long-range correlation between hadrons produced in the CFR and the TFR. The resulting beam-spin asymmetry

¹ We use the standard definition for Feynman variables x_{F1} and x_{F2} , see next section.

contains the convolution of the fracture function and the fragmentation function modulated by $\sin \Delta\phi$,

$$\mathcal{A}_{LU} = -\sqrt{1-\epsilon^2} \frac{|\vec{P}_{T1}||\vec{P}_{T2}|}{m_N m_2} \frac{\mathcal{C}[w_5 \hat{l}_1^{\perp h} D_1]}{\mathcal{C}[\hat{u}_1 D_1]} \sin \Delta\phi. \quad (3)$$

The depolarization factor in the front of Eq. 3, governing the polarization transfer from the electron to virtual photon, is described by the variable

$$\epsilon = \frac{1-y-\frac{1}{4}\gamma^2 y^2}{1-y+\frac{1}{2}y^2+\frac{1}{4}\gamma^2 y^2}, \quad (4)$$

with $\gamma = 2m_N x/Q$. The weight factor is given by

$$w_5 = \frac{(\vec{k}_\perp \cdot \vec{P}_{T2})(\vec{P}_{T1} \cdot \vec{P}_{T2}) - (\vec{k}_\perp \cdot \vec{P}_{T1})\vec{P}_{T2}^2}{(\vec{P}_{T1} \cdot \vec{P}_{T2})^2 - \vec{P}_{T1}^2 \vec{P}_{T2}^2}, \quad (5)$$

and the following notation is used for the transverse momentum convolution

$$\mathcal{C}[f(\vec{k}_\perp, \vec{k}'_\perp, \dots)] = \sum_a e_a^2 x_B \int d^2 \vec{k}_\perp \int d^2 \vec{k}'_\perp \times \delta^2(\vec{k}_\perp - \vec{k}'_\perp - \vec{P}_{T1}/z_1) f(\vec{k}_\perp, \vec{k}'_\perp, \dots), \quad (6)$$

where k_\perp is the transverse momentum of the initial quark with respect to the virtual photon, k'_\perp is the transverse momentum after the interaction and the summation runs over the quark flavors.

EXPERIMENT

The data, corresponding to SIDIS events with a π^+ the CFR and proton in the TFR, were taken in two run periods in the fall of 2018 and spring 2019 using 10.6 and 10.2 GeV longitudinally polarized electron beams delivered by the Continuous Electron Beam Accelerator Facility at Jefferson Lab [22]. The electron beam was incident on a liquid-hydrogen target and reactions were recorded using the CLAS12 spectrometer [9]. The beam polarization averaged to $85.7 \pm 1.6\%$ and was flipped at a rate of 30 Hz to minimize systematic effects.

A tracking subsystem consisting of drift chambers in a toroidal magnetic field was used to identify and reconstruct particles scattered in the forward direction. A high-threshold Cherenkov counter was used to distinguish between electrons and final-state hadrons. Additional identification criteria for the electrons was also imposed using a series of electromagnetic calorimeters. The CLAS12 forward time-of-flight systems, composed of six arrays of plastic scintillation counters, were used to analyze the velocity vs. momentum relationship of positive tracks to distinguish between hadron species. The pions were limited to momenta $1.2 < p < 4.0$ GeV in order to avoid regions of low efficiency (lower limit) and minimize misidentification of kaons (upper limit). Protons were

required to have a momentum greater than 0.5 GeV (no strict upper limit was enforced but the distribution of upper proton momenta dies down around 2.5 GeV, well before any significant contamination from lighter hadron species). The reconstructed electron and hadrons were required to have been identified in the so-called “forward detector” of CLAS12 and a requirement has been placed on the polar angle of each track, $\theta < 30^\circ$.

SIDIS events were selected with the usual requirement that $Q^2 > 1$ GeV² and the mass of the hadronic final-state, $W > 2$ GeV. Events with a radiated photon were limited by requiring events to have $y < 0.75$. At energies accessible by fixed target experiments there is no rapidity gap and the forward and backward regions were defined by the variable x_F , in the virtual photon-nucleon center-of-mass frame, with the requirement that $x_{F1} > 0$ and $x_{F2} < 0$. The Feynman- x variable is defined as $x_{F1(2)} = 2P_{\parallel 1(2)}/W$, where P_{\parallel} is the longitudinal momentum of the hadron and takes a positive value if the hadron moves in the same direction as the momentum transfer dictated by virtual photon and a negative value if it moves in the same direction of the target in the center-of-mass frame. An additional requirement on the boost-invariant quantity $\Delta Y \equiv Y_1 - Y_2 > 0$, where Y is the rapidity evaluated in the Breit frame defined as $2Y_{1(2)} = \ln(E_{1(2)} + P_{\parallel 1(2)})/(E_{1(2)} - P_{\parallel 1(2)})$, was required to enforce separation between the hadrons. The asymmetries were studied as a function of both of these variables to investigate the transition from one region to another. Contributions from Δ^{++} decays were minimized by requiring the invariant mass of the observed hadrons to have $M_{p\pi} > 1.5$ GeV. Finally, the missing mass of the process $ep \rightarrow e'p\pi^+X$ was restricted to be greater than 0.95 GeV in order to avoid contributions from diffractive meson production.

RESULTS

The beam-spin asymmetry can be accessed using the yields, N^\pm , of events with a proton in the backward region and a positive pion in the forward region, produced from the scattering of an electron with helicity \pm , written

$$\mathcal{A}_{LU}(\Delta\phi) = \frac{1}{P_{\text{beam}}} \frac{N^+(\Delta\phi) - N^-(\Delta\phi)}{N^+(\Delta\phi) + N^-(\Delta\phi)} = \quad (7)$$

$$\mathcal{A}_{LU}^{\sin(\Delta\phi)} \sin(\Delta\phi) + \mathcal{A}_{LU}^{\sin(2\Delta\phi)} \sin(2\Delta\phi),$$

with the dependence on $\sin(\Delta\phi)$ and $\sin(2\Delta\phi)$ described in Ref. [20], and fitting for the resulting azimuthal modulation amplitudes. The beam polarization, P_{beam} , has been divided out of the asymmetries. The amplitudes in Eq. (7) were extracted from the data using an unbinned maximum likelihood fit that includes both modulations of \mathcal{A}_{LU} . A binned χ^2 -minimization fit with 9 bins in $\Delta\phi$ was also performed and is in very good agreement

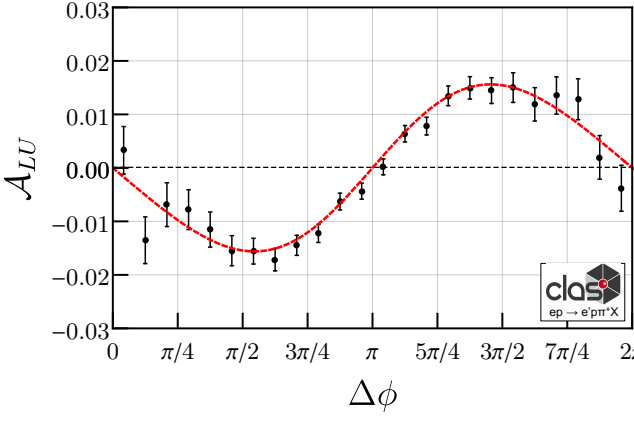


FIG. 2. The beam spin asymmetry, \mathcal{A}_{LU} , as a function of $\Delta\phi$ and integrated over all other kinematics for the entire data set. A clear $\sin(\Delta\phi)$ dependence is observed with small $\sin(2\Delta\phi)$ contributions.

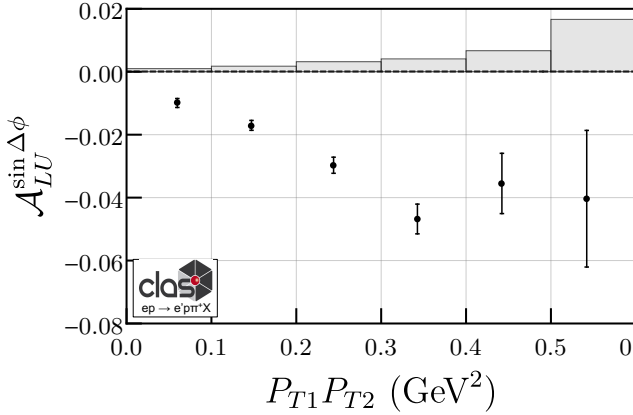


FIG. 3. The measured $\mathcal{A}_{LU}^{\sin \Delta\phi}$ asymmetry as a function of $P_{T1}P_{T2}$. Thin black bars indicate statistical uncertainties and wide gray bars represent systematic uncertainties.

with the unbinned fit with a mean reduced χ^2 of 1.01. The count-rate asymmetry between positive and negative electron helicities as a function of $\Delta\phi$ is shown in Fig. 2. The count rate difference exhibits a clear $\sin(\Delta\phi)$ behavior with a much smaller $\sin(2\Delta\phi)$ contribution.

The dependence of $\mathcal{A}_{LU}^{\sin \Delta\phi}$ on the product of transverse momenta of the proton and pion is shown in Fig. 3 and is consistent with a linear increase in magnitude and approaches zero as the transverse momentum goes to zero, following the kinematic dependence predicted by theory (see. Eq. 3). Additional multidimensional asymmetries as a function of the product of the transverse momenta in bins of z_1 are given in the supplementary material.

Due to the correlation between different kinematic variables and the product of the transverse momenta of both hadrons, the asymmetries can be weighted by dividing out the depolarization and kinematic weighting factor

in Eq. 3, $\sqrt{1 - \epsilon^2}(P_{T1}P_{T2})/(m_N m_2)$, (note that for this measurement $m_N = m_2 = 0.938$ GeV). The dependence of the resulting ratio, which should directly depend on the ratio of the convolutions of fracture and fragmentation functions, was studied for several different kinematic variables.

The x -dependence, shown in Fig. 4, has the general trend of increasing in magnitude as x increases. This strong dependence implies that the correlation of final-states hadrons is most significant in the valence quark region. The dependence on z_1 of the pion, which reflects the fragmentation function dependence, is shown in Fig. 5. At relatively small z_1 , contributions from the initial quark transverse momentum can be neglected and the main contribution to the produced hadron transverse momentum comes from the struck quark hadronization process. Indeed, this dependence appears relatively flat, with a possible decrease at higher values of z_1 where effects from decreasing transverse momentum begin to dominate. This relatively weak dependence may also be a consequence of cancellation between the pion fragmentation functions in the numerator and denominator. The dependence on ζ_2 , shown in Fig. 6, is stronger and may be interpreted in terms of strong correlations with other variables such as x ; typically the higher longitudinal momentum carried by the struck quark, the lower the longitudinal momentum available for the TFR hadron.

Additional kinematic dependences are included in the supplementary material. The asymmetries plotted versus x_{F1} and ΔY (with the kinematic constraints on x_{F2} , x_{F1} and ΔY removed) show a relatively flat dependence in the $x_{F1} < 0$ region with a possible transition in the positive region where the proton is increasingly likely to have originated in the CFR and the back-to-back fracture function formalism no longer holds. Finally, the dependence on the missing mass, with the $M_x > 0.9$ GeV requirement removed, shows a relatively flat behavior above the contributions from diffractive $ep \rightarrow e'\pi^+\pi^-$ and $ep \rightarrow e'\pi^+\rho^-$ events.

Relevant systematic uncertainties have been estimated using a number of methods. Monte Carlo simulations were performed using the PEPSI generator [23] and a GEANT4-based simulation [24, 25] of the detector for acceptance, efficiency and particle-ID studies. Good agreement for all underlying variables was observed. Systematic uncertainties due to bin migration and the scale uncertainty on the beam polarization can reach a few percent in each bin. Other effects due to particle misidentification, accidental coincidences, photoproduction of electrons and contamination from target-fragmentation pions (baryonic decays like $\Delta^{++} \rightarrow p\pi^+$) have all been estimated to be small. Contributions from radiative effects are avoided by limiting our kinematic range and are also thought to be small. However, it is possible that this has been underestimated due to the lack of theory available for radiative effects in SIDIS.

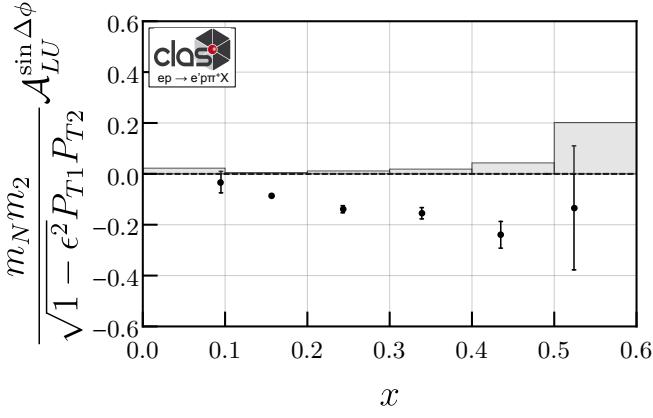


FIG. 4. The measured weighted $A_{LU}^{\sin \Delta \phi}$ asymmetry as a function of x . Thin black bars indicate statistical uncertainties and wide gray bars represent systematic uncertainties.

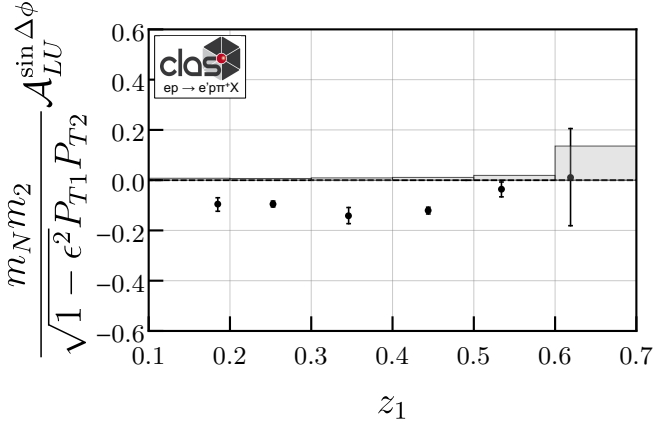


FIG. 5. The measured weighted $A_{LU}^{\sin \Delta \phi}$ asymmetry as a function of z_1 . Thin black bars indicate statistical uncertainties and wide gray bars represent systematic uncertainties.

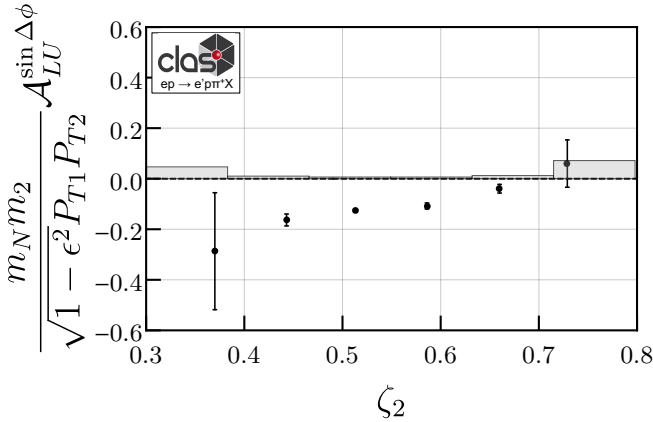


FIG. 6. The measured weighted $A_{LU}^{\sin \Delta \phi}$ asymmetry as a function of ζ_2 . Thin black bars indicate statistical uncertainties and wide gray bars represent systematic uncertainties.

The largest systematic uncertainty comes from contributions from the unpolarized cross section. After integration over ϕ_2 , the only remaining structure functions are F_{UU} and $F_{LU}^{\sin(\Delta\phi)}$. However, due to the non-perfect acceptance of CLAS12 and the potential resulting non-orthogonality of modulations, the other unpolarized structure functions may impact our extraction of the F_{LU} amplitudes. Since there is no experimental data on the spin-independent (UU) modulations, the uncertainty due to not including these modulations in our fit has been evaluated using Monte Carlo simulations by injecting various values of the amplitudes and then performing fits not including the UU modulations in order to measure the possible deviation in our LU amplitudes. The effect is heavily bin-dependent, but can only reach magnitudes similar to the statistical uncertainty at edges of kinematic space. For example, in the lowest x -bin we assign an uncertainty to $A_{LU}^{\sin \Delta \phi}$ of 0.006 compared to 0.021 at the highest x bin where the measurement is less constrained. This study is both dependent on our injected amplitudes and fairly conservative and so, therefore, may correspond to an overestimate.

CONCLUSIONS

In summary, the kinematic dependences of beam SSAs in the production of two hadrons in opposite hemispheres have been measured for the first time. The asymmetries may be interpreted in a framework described by TMD factorization into fracture functions and fragmentation functions, with the conditional probability of finding a proton originating from the target remnant after the emission of a quark which undergoes hadronization to form a final-state π^+ . The P_T dependence of the asymmetries is consistent with predictions of the factorized framework and can ultimately be used to test TMD factorization once extractions of the relevant functions are available and predictions have been made.

Our measurement of correlations between the target- and current-fragmentation regions develop a new methodology to quantify the relationship between the spin and transverse momenta of quarks in the nucleon and provides a new avenue for studies of the complex nucleonic structure in terms of quark and gluon degrees of freedom. The kinematics of the generated asymmetries are not in the perturbative regime, but instead, the asymmetries likely originate from correlations between the longitudinally polarized struck quark's azimuthal angle and the azimuthal angle of the proton produced in the TFR [7].

Future work will extend the analysis to other hadron species in both the TFR and CFR in order to test the universal nature of fracture functions. The flavor dependence of fracture functions can be extracted by comparing with deuterium targets, of which compara-

ble statistics to the proton-target data shown here have already been collected by CLAS12. Finally, polarized target measurements will enable access to the complete set of leading-twist fracture functions, which cannot be observed in single-hadron production but require an additional hadron to produced in the CFR like the measurement performed here.

ACKNOWLEDGEMENTS

We acknowledge the outstanding efforts of the staff of the Accelerator and the Physics Divisions at Jefferson Lab in making this experiment possible. This work was supported in part by the U.S. Department of Energy, the National Science Foundation (NSF), the Italian Istituto Nazionale di Fisica Nucleare (INFN), the French Centre National de la Recherche Scientifique (CNRS), the French Commissariat pour l'Energie Atomique, the UK Science and Technology Facilities Council, the National Research Foundation (NRF) of Korea, the Helmholtz-Forschungsakademie Hessen für FAIR (HFHF), the Ministry of Science and Higher Education of the Russian Federation, the Chilean Agencia Nacional de Investigación y Desarrollo (ANID) via grant PIA/APOYO AFB180002 and the European Union's Horizon 2020 Research and Innovation program under Grant Agreement N.824093 (STRONG2020). The Southeastern Universities Research Association (SURA) operates the Thomas Jefferson National Accelerator Facility for the U.S. Department of Energy under Contract No. DE-AC05-06OR23177. The work is also supported in part by DOE grant DE-FG02-04ER41309.

-
- [1] M. Anselmino, A. Mukherjee, and A. Vossen, *Prog. Part. Nucl. Phys.* **114**, 103806 (2020), arXiv:2001.05415 [hep-ph].
 - [2] A. Bacchetta, M. Diehl, K. Goeke, A. Metz, P. J. Mulders, and M. Schlegel, *JHEP* **02**, 093, arXiv:hep-ph/0611265.
 - [3] J. Gao, L. Harland-Lang, and J. Rojo, *Phys. Rept.* **742**, 1 (2018), arXiv:1709.04922 [hep-ph].
 - [4] J. J. Ethier and E. R. Nocera, *Ann. Rev. Nucl. Part. Sci.* **70**, 43 (2020), arXiv:2001.07722 [hep-ph].
 - [5] A. Metz and A. Vossen, *Prog. Part. Nucl. Phys.* **91**, 136 (2016), arXiv:1607.02521 [hep-ex].
 - [6] L. Trentadue and G. Veneziano, *Phys. Lett.* **B323**, 201 (1994).
 - [7] M. Anselmino, V. Barone, and A. Kotzinian, *Phys. Lett.* **B699**, 108 (2011), arXiv:1102.4214 [hep-ph].
 - [8] M. Anselmino, V. Barone, and A. Kotzinian, *Phys. Lett.* **B706**, 46 (2011), arXiv:1109.1132 [hep-ph].
 - [9] V. D. Burkert *et al.* (CLAS Collaboration), *Nucl. Instrum. Meth. A* **959**, 163419 (2020).
 - [10] H. Avakian and S. Pisano, *Proceedings, 24th International Workshop on Deep-Inelastic Scattering and Related Subjects (DIS 2016): Hamburg, Germany, April 11-15, 2016*, PoS **DIS2016**, 214 (2016).
 - [11] H. Avakian *et al.* (CLAS), *Phys. Rev. D* **69**, 112004 (2004), arXiv:hep-ex/0301005.
 - [12] S. Diehl *et al.* (CLAS Collaboration), *Phys. Rev. Lett.* **128**, 062005 (2022), arXiv:2101.03544 [hep-ex].
 - [13] M. Mirazita *et al.* (CLAS Collaboration), *Phys. Rev. Lett.* **126**, 062002 (2021), arXiv:2010.09544 [hep-ex].
 - [14] T. B. Hayward *et al.* (CLAS Collaboration), *Phys. Rev. Lett.* **126**, 152501 (2021), arXiv:2101.04842 [hep-ex].
 - [15] A. Airapetian *et al.* (HERMES Collaboration), *Phys. Lett.* **B648**, 164 (2007), arXiv:hep-ex/0612059.
 - [16] C. Adolph *et al.* (COMPASS Collaboration), *Nucl. Phys. B* **886**, 1046 (2014), arXiv:1401.6284 [hep-ex].
 - [17] B. Parsamyan, *Proceedings, 25th International Workshop on Deep-Inelastic Scattering and Related Topics (DIS 2017): Birmingham, UK, April 3-7, 2017*, **DIS2017**, 259 (2018), arXiv:1801.01488 [hep-ex].
 - [18] B. Parsamyan, *Proceedings, QCD Evolution Workshop (QCD 2017): Newport News, VA, USA, May 22-26, 2017*, PoS **QCDEV2017**, 042 (2018).
 - [19] R. L. Jaffe, H. Meyer, and G. Piller, *Lect. Notes Phys.* **496**, 178 (1997).
 - [20] M. Anselmino, V. Barone, and A. Kotzinian, *Phys. Lett. B* **713**, 317 (2012), arXiv:1112.2604 [hep-ph].
 - [21] M. Anselmino, V. Barone, and A. Kotzinian, *Phys. Lett. B* **713**, 317 (2012), arXiv:1112.2604 [hep-ph].
 - [22] C. W. Leemann, D. R. Douglas, and G. A. Krafft, *Ann. Rev. Nucl. Part. Sci.* **51**, 413 (2001).
 - [23] L. Mankiewicz, A. Schafer, and M. Veltri, *Comput. Phys. Commun.* **71**, 305 (1992).
 - [24] S. Agostinelli *et al.* (GEANT4), *Nucl. Instrum. Meth. A* **506**, 250 (2003).
 - [25] M. Ungaro *et al.*, *Nucl. Instrum. Meth. A* **959**, 163422 (2020).